

The EBEX Experiment

P. Oxley^a, P. Ade^b, C. Baccigalupi^c, P. deBernardis^d, H-M. Cho^e, M. J. Devlin^f, S. Hanany^a,
 B. R. Johnson^a, T. Jones^a, A. T. Lee^{e,g}, T. Matsumura^a, A. D. Miller^h, M. Milligan^a,
 T. Renbarger^a, H. G. Spieler^g, R. Stomporⁱ, G. S. Tucker^j, M. Zaldarriaga^k

^a Dept. of Physics and Astronomy, University of Minnesota, Minneapolis, MN 55455, U.S.A.;

^b Dept. of Physics and Astronomy, University of Wales, Cardiff, CF24 3YB, Wales;

^c International School for Advanced Studies, 34014 Trieste, Italy;

^d Dipartimento di Fisica, Universita di Roma La Sapienza, 00185 Rome, Italy;

^e Dept. of Physics, University of California, Berkeley, CA 94720, U.S.A.;

^f Dept. of Physics, University of Pennsylvania, Philadelphia, PA 19104, U.S.A.;

^g Physics Division, Lawrence Berkeley Nat. Lab., Berkeley, CA 94720, U.S.A.;

^h Dept. of Physics, Columbia University, New York, NY 10027, U.S.A.;

ⁱ Computational Research Division, Lawrence Berkeley Nat. Lab., Berkeley, CA 94720, U.S.A.;

^j Dept. of Physics, Brown University, Providence, RI 02912, U.S.A.;

^k Astronomy Department, Harvard University, Cambridge, MA 02138, U.S.A.;

ABSTRACT

EBEX is a balloon-borne polarimeter designed to measure the intensity and polarization of the cosmic microwave background radiation. The measurements would probe the inflationary epoch that took place shortly after the big bang and would significantly improve constraints on the values of several cosmological parameters. EBEX is unique in its broad frequency coverage and in its ability to provide critical information about the level of polarized Galactic foregrounds which will be necessary for all future CMB polarization experiments.

EBEX consists of a 1.5 m Dragone-type telescope that provides a resolution of less than 8 arcminutes over four focal planes each of 4° diffraction limited field of view at frequencies up to 450 GHz. The experiment is designed to accommodate 330 transition edge bolometric detectors per focal plane, for a total of up to 1320 detectors. EBEX will operate with frequency bands centered at 150, 250, 350, and 450 GHz. Polarimetry is achieved with a rotating achromatic half-wave plate. EBEX is currently in the design and construction phase, and first light is scheduled for 2008.

Keywords: EBEX, CMB, TES, bolometers, polarimetry, magnetic bearing

1. INTRODUCTION

EBEX (E and B EXperiment) is a long duration balloon-borne experiment equipped with arrays of hundreds of bolometric transition edge sensors (TES) at the focal plane of a 1.5 m aperture telescope. It will measure the temperature and polarization of the cosmic microwave background (CMB) radiation. EBEX has four primary scientific goals, (1) to detect the B-mode inflationary gravitational-wave background signal, or set an upper bound that is a factor of ~ 15 more restrictive than current bounds, (2) to provide critical information about the polarization of Galactic foregrounds, particularly of dust emission, at the micro-Kelvin level, (3) to measure the yet undetected signature of lensing of the polarization of the CMB, and (4) to improve the determination of several cosmological parameters by up to a factor of six. All of these goals are of fundamental importance for physics and astrophysics. EBEX will provide an important milestone in the implementation and testing of detector, detector readout, optics, and polarimetry techniques that are being considered for a future NASA CMB polarization satellite, and is unique in its foreground determination capability compared to all current and proposed CMB experiments. In Sec. 2 we review the cosmology that will be probed with the EBEX measurements and in Sec. 3 we describe the EBEX instrument.

Send correspondence to P. Oxley: E-mail: oxley@physics.umn.edu, Telephone: +1 612 624 0673

2. SCIENCE

Since its discovery in 1965 the cosmic microwave background radiation has been one of the pillars of the Big Bang model.¹ Measurements of its spectrum firmly established the hot big bang model as the basis of our understanding of cosmology.² Measurements of the anisotropy of the CMB over the last fifteen years have enabled us to determine cosmological parameters such as the age, density and composition of the universe^{3,4} to unprecedented accuracy. Recent measurements of the polarization of the CMB provide strong support for our model of the CMB.^{5,6}

As a result of these and other astrophysical observations we have a very successful model for how structures have formed in our universe. Gravitational instability makes fluctuations grow with time, but the fluctuations require initial seeds. The CMB temperature power spectrum and the angular dependence of the cross-correlation between temperature and polarization⁷ imply that these seeds had to be created very early in the evolution of the universe.⁸⁻¹⁰

The leading scenario for the creation of the primordial seeds is the paradigm of inflation.¹¹⁻¹⁴ The fluctuations we see today are the direct result of quantum fluctuations of a very light scalar field, the inflaton, during a period of accelerated expansion or “inflation”, a small fraction of a second after the big bang.¹⁵⁻²¹ However, many of the details of the inflationary scenario are uncertain and perhaps more importantly, the paradigm currently lacks any strong confirmation.

A promising way to confirm the inflationary scenario is via its prediction of a stochastic background of gravity waves,^{18,19,22-24} which we call the inflationary gravitational-wave background (IGB). The best known way to search for the IGB is through its signature on the CMB polarization.^{25,26} Thomson scattering of an anisotropic radiation field leads to linear polarization. The temperature anisotropy produced by density perturbations and by gravity waves both lead to linear polarization through this mechanism. However, the pattern of the induced polarization on the sky should be very different in each case. Density perturbations produce a curl-free or E-mode pattern of polarization vectors. Gravity waves produce a curl or B-mode pattern of polarization vectors that density perturbations cannot produce.^{27,28} Thus if polarization can be mapped and decomposed into E and B components (Fig. 1, left panel), the B component will be an unambiguous signature of the IGB and therefore for inflation. Detection of this IGB signal is a primary goal of the EBEX experiment.

The IGB signal is extremely faint – with a similar or smaller amplitude than expected foreground signals. It is anticipated that the most significant foreground signal will be from polarized Galactic dust²⁹ (Fig. 1, left panel). However, there is currently very little information about the level of polarized dust and its orientation as a function of position on the sky, or about its E and B power spectra. No information exists for any region of the sky at the accuracies required for a B-mode signal detection. A primary goal of EBEX will be to characterize the polarized dust emission and determine its angular power spectra in both E and B-type polarizations.

The dust signal increases with increasing frequency, while the CMB signal is at a maximum at ≈ 150 GHz. The measurements at 250, 350, and 450 GHz will be primarily sensitive to dust emission, and by extrapolating these measurements to 150 GHz the dust foreground will be subtracted from the primary CMB band at 150 GHz. The predicted uncertainty in the determination of the dust signal at 150 GHz is shown in the right panel of Fig. 1. The dust measurements will also provide the community with critical information about the polarized dust fraction and orientation as a function of frequency. Given the expected magnitude of the polarized dust foreground, this information is essential for *all* future CMB polarization experiments.

We have chosen a balloon-borne platform for EBEX because this allows measurements over a broad frequency range and reduces atmospheric effects by three orders of magnitude.³² At frequencies higher than ~ 150 GHz atmospheric emission becomes significant and broad-band observations from the ground are difficult because of a combination of lower detector sensitivity (a result of increased incident power) and higher noise (due to fluctuations in sky emission). Broad-band, ground-based observations are essentially impossible from anywhere on Earth at the higher frequency bands. EBEX is unique among CMB polarization experiments in that it will have four frequency bands between 150 and 450 GHz. This is the broadest frequency coverage of all current and proposed bolometric CMB polarimeters and gives EBEX an unprecedented capability to measure the polarization of the dust emission (Fig. 1, right panel).

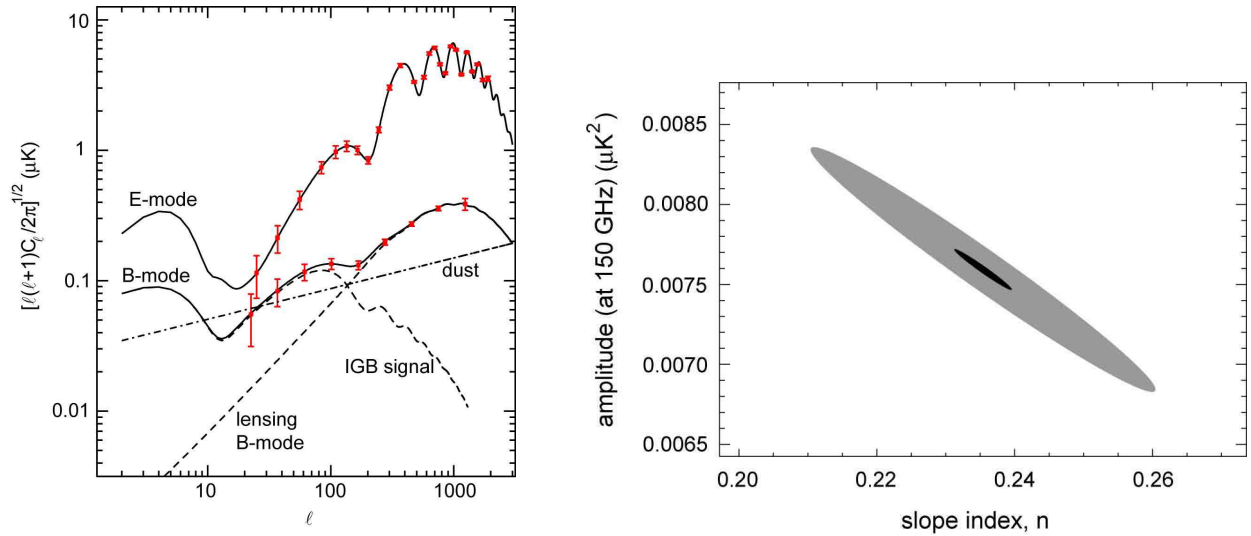


Figure 1. Left panel: The angular power spectrum of the CMB E and B-mode signal at 150 GHz (solid lines). The B-mode signal is the sum of contributions from lensing and the IGB (dashed lines) in a Λ CDM cosmological model with the amplitude of the IGB signal a factor of five lower than current upper limits. The x-axis is spherical multipole moment ℓ . The data points represent the expected performance of EBEX after a 14 day flight in Antarctica.³⁰ Also shown is the estimated dust foreground angular power spectrum at 150 GHz for the region of the sky to be scanned by EBEX. The dust foreground shown is the same in both E and B-type polarization patterns, and its amplitude and slope will be determined by EBEX measurements at 250, 350, and 450 GHz. Right panel: Two sigma uncertainty ellipses in EBEX determination of the amplitude and angular power spectrum slope of the 150 GHz B-mode power spectrum from dust. With 55, 30, and 25 detectors at 250, 350, and 450 GHz, respectively, and for a 14 day flight, the amplitude and slope will be determined to 6% (lighter colored ellipse). With 330, 180, and 150 detectors at these frequencies the two sigma uncertainty is 1% (darker colored ellipse). Nominal values of $0.00759 \mu\text{K}^2$ and 0.235 for the amplitude and slope are used.³¹

The atmosphere is a source of polarized intensity because of Zeeman-splitting of rotational levels of oxygen. The levels are split by the Earth’s magnetic field and the amount and orientation of the polarized intensity depends on the strength and direction of the field.^{32,33} The atmospheric linear polarization is predicted to occur at only the $\sim 10^{-9}$ K level, but circular polarization is predicted at a level of $\sim 100 \mu\text{K}$.³² A conversion of circular to linear polarization in any ground-based instrument with a level as low as 0.1% would give rise to an instrumental polarization signal that is approximately as large as the IGB signal of $0.1 \mu\text{K}$ shown in Fig 1, left panel. At 90 GHz the atmospheric signal is ~ 5 times the IGB signal. At balloon altitudes the atmospheric signal is a factor of 1000 smaller and therefore should be negligible for EBEX.

Gravitational lensing of CMB photons along their path gives rise to an additional effective foreground. The lensing is the result of the deflection of the path of CMB photons by intermediate mass and energy structures, and it creates a B-mode polarization pattern even in the absence of gravity waves.³⁴ Based on current measurements of cosmological parameters the magnitude of the lensing B signal is predicted with $\sim 20\%$ uncertainty,^{3,4} but because of its low amplitude it has not yet been detected. If the amplitude of the lensing signal agrees with predictions, EBEX should have the combination of sensitivity and angular resolution to detect and constrain its amplitude to within 4%. If EBEX achieves its predicted sensitivity a “no-detection” would be of substantial importance because it would require major revisions of our understanding of the evolution of the universe.

EBEX should make a high signal-to-noise ratio determination of the CMB temperature and the E-mode polarization spectrum, and the spectrum of the correlation between the two. The E-mode measurement will allow a factor of between two and three improvement in current estimates of the density of dark energy, the density of dark matter, the density of baryonic matter, and the amplitude of the primordial density fluctuations spectrum. The spatial distribution of density perturbations in the early universe is parameterized by their spectral index and EBEX should improve current constraints on the running of this spectral index by a factor of six.

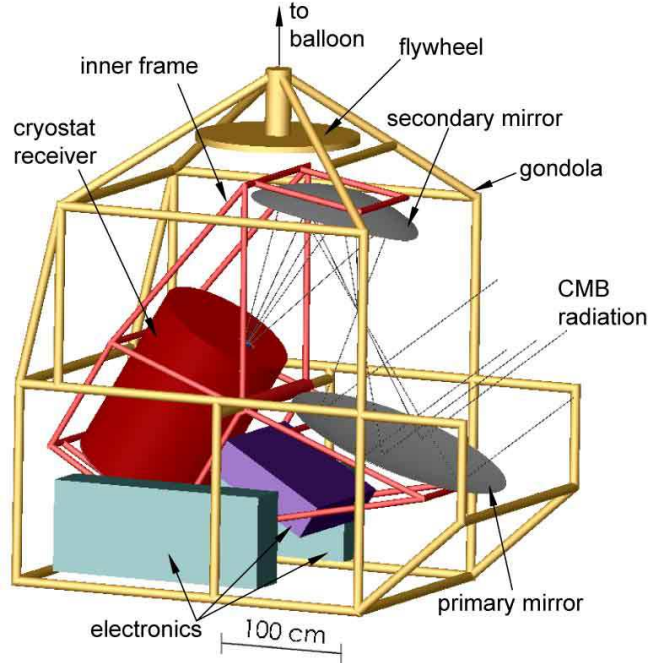


Figure 2. Solid model of the EBEX experiment and balloon gondola showing the telescope primary and secondary mirrors and the cryostat which contains re-imaging optics and the TES detectors.

3. EXPERIMENTAL DETAILS

3.1. Summary of Approach

EBEX will employ a 1.5 m telescope to focus radiation on up to four separate focal planes, each containing up to 330 TES spider web bolometers cooled to 300 mK. The experiment will operate at four frequency bands, centered on 150, 250, 350, and 450 GHz. The unpolarized (T) and linearly polarized (Q and U) Stokes parameters of the CMB radiation will be measured by the well-tested technique of rotating an achromatic half-wave plate at the aperture stop of the telescope and analyzing the radiation with a wire grid polarizer. The telescope will scan a patch of sky 350 deg^2 with a resolution of 8 arcminutes at 150 GHz (Table 1).

EBEX is carefully optimized to achieve its science goals. The balloon-borne platform and the broad frequency coverage will provide critical information about the dust foreground. The large number of detectors will give the required combined sensitivity that will allow detection of the IGB signal. Figure 2 shows the EBEX payload.

3.1.1. Detectors and Readout

The detection of the IGB signal requires high sensitivity. However, detector technologies have matured to the point that the noise of a bolometric detector is dominated by noise in the background optical loading and therefore the sensitivity of a single detector cannot be improved. To improve sensitivity it is essential to implement arrays of detectors.

We have chosen to use arrays of transition edge sensors for EBEX for several compelling reasons. They are produced by thin film deposition and optical lithography, which is ideal for producing large detector arrays. Due to a strong negative electrothermal feedback effect, they are extremely linear and the responsivity is determined only by the bias voltage, insensitive to fluctuations in the incident optical power and bath temperature. The electrothermal feedback also strongly reduces Johnson and $1/f$ noise in the TES. TES bolometers are low-impedance devices, which results in a lower vibration sensitivity than that of high-impedance semiconductor bolometer technologies. SQUID amplifiers will be used to read out the TES bolometers. These amplifiers are inherently low noise devices and there is the possibility to use multiplexed SQUID amplifiers, which will simplify our cryogenic design and facilitate the use of the full 1320 detector capability of EBEX.

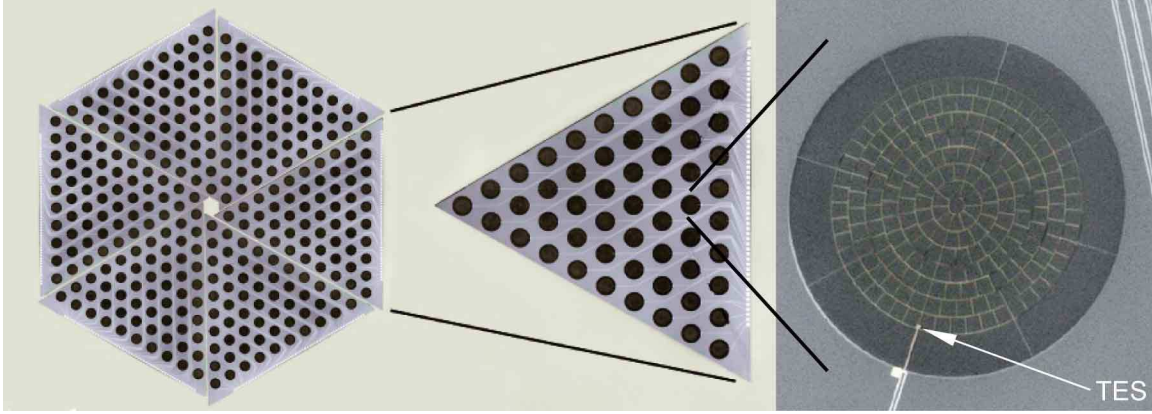


Figure 3. Left panel: Montage image of a photograph of a single real TES “wedge” of spider bolometers replicated electronically to show how a final array will look. Each wedge is designed to be identical and has 55 bolometers. The entire array will have 330 bolometers and be 17 cm in diameter. Center panel: Photograph of wedge of 55 spider web TES bolometers. Wedge is 8 cm on a side. Suspended spider web absorbers are fabricated from $1\ \mu\text{m}$ thick silicon nitride. The membrane is released from the front side using a gaseous xenon difluoride etch. Bolometers are 3.5 mm diameter with 0.5 mm long legs. Wiring layer is superconducting aluminum. This array was fabricated in the U.C. Berkeley microfabrication facility. Right panel: Close up of 55 element bolometer wedge. Sensors are an Al/Ti proximity effect sandwich TES, located at the edge of the membrane and electrically connected with superconducting leads.

In our TES spider web bolometer CMB radiation is absorbed by a metalized silicon nitride mesh in a pattern similar to that of a spider’s web (Fig. 3, right panel). EBEX will use arrays of 55 TES bolometers fabricated by our collaborators at UC Berkeley using standard microlithographic techniques. A 330 element TES array is built by tiling six 55 element arrays (Fig. 3, left panel) and will fill the EBEX focal plane. The arrays are identical in many of their construction parameters to the arrays that will be used for the ground-based experiment APEX³⁵ and for the South-Pole Telescope (SPT).³⁶ However, compared to the APEX TES the thermal conductance of the EBEX TES will be reduced to $10\ \text{pWK}^{-1}$ to match the lower optical loading at balloon altitudes.

The responsivity, noise properties and time constants of individual TES bolometers have been studied extensively.^{37–41} The measured noise has been shown to reach the fundamental thermal-fluctuation noise limit (Fig. 4), and the responsivities and time constants match theory closely. Table 1 gives the expected noise equivalent power (NEP) of the EBEX detectors at each frequency.

Initially EBEX will use individual SQUIDs to read the current from each TES bolometer using the readout technique that has been developed for the APEX and SPT receivers. This technique uses a single series-array SQUID coupled to a single room-temperature op-amp. The TES bolometer is ac-biased with a direct-digital synthesis generator and the signal is demodulated with an analog mixer circuit. Since SQUIDs are sensitive to stray magnetic fields the TES and SQUID will be enclosed in a Cryoperm shield.

The above readout system is fully compatible with the frequency-domain multiplexing readout that is being developed by our collaborators at UC Berkeley and Lawrence Berkeley National Lab. The principle of this technique has already been demonstrated by monitoring the current passing through 8 mock TES.⁴² Two real TES have also been multiplexed⁴³ and experiments are underway to further test the technique with greater numbers of TES bolometers. With multiplexed readouts we will use one SQUID readout circuit to read 20 detectors, thereby reducing the number of SQUID wires reaching cryogenic temperatures by the same factor. This substantially reduces the heat load on the cryostat allowing use of the full 1320 detector capability of EBEX. When individual SQUIDs are used to read out each TES the number of detectors will be limited to 715, distributed between the four focal planes. Multiplexed readouts will allow more detectors to be allocated to the 250, 350, and 450 GHz frequency bands, improving the determination of the dust foreground compared to the case of non-multiplexed readouts (Fig. 1, right panel).

The TES bolometers will operate from a bath temperature of $\sim 300\ \text{mK}$ provided by a ^3He fridge. The fridge will work off of a standard liquid helium/liquid nitrogen cryostat with two vapor cooled shields connected to

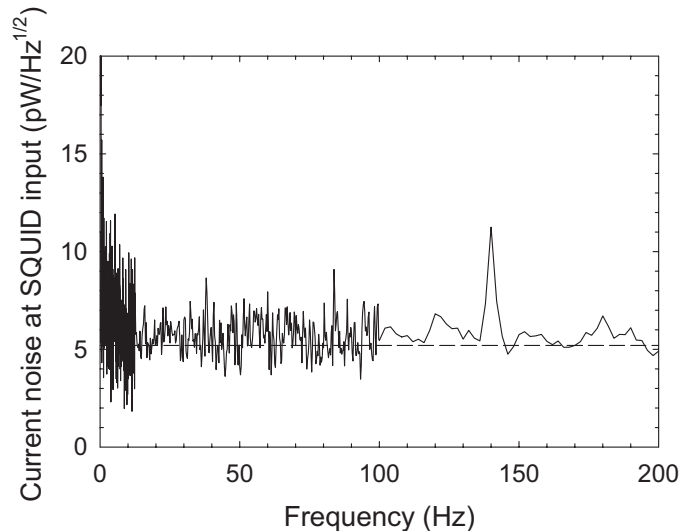


Figure 4. Noise performance of an individual spider web TES bolometer with no incident optical power. The noise is at the fundamental thermal noise limit as indicated by the horizontal dashed line, and the time constant is 0.6 ms. The feature at 140 Hz is a mechanical resonance of the table upon which the bolometer is mounted.

Table 1. Expected TES noise and angular resolution for EBEX. The TES noise is dominated by photon and thermal noise. Photon noise is due to fluctuations in the number of CMB photons arriving at the TES and thermal noise is caused by fluctuations in the number of phonons in the heat link between the TES and the low temperature bath used to cool the TES. The angular resolution is determined by the telescope 1.5 m aperture primary mirror.

Frequency (GHz)	NEP $\times 10^{-17} \text{ WHz}^{-1/2}$	Angular Resolution (FWHM, arcminutes)
150	1.12	8
250	1.28	4.8
350	1.48	3.4
450	1.71	2.7

the boil-off gases of each of the liquids. A detailed thermal model of the cryostat has been made, including all anticipated major heat loads such as radiation, wires, heat load through the 15 cm diameter cryostat window, and parasitic heat loads on the different thermal stages. The modelling predicts that 105 l of liquid helium and 140 l of liquid nitrogen will be sufficient for a hold time of 20 days.

3.1.2. Telescope and Cold Optics

The EBEX optical system is based on the existing well-characterized telescope from the Archeops experiment. It consists of the Archeops 1.5 m aperture primary mirror and a new 1.2 m elliptical secondary that together make a Dragone telescope (Fig. 5, left panel). This design provides a 4° field of view and beam resolutions given in Table 1.

Figure 5, right panel, shows the optics of EBEX contained within the cryostat receiver of Fig. 2. Four cold lenses, a dichroic filter and two polarizing grids couple radiation from the telescope into four independent focal planes. The lenses, which will be made of either silicon or high density polyethylene, provide both a cold aperture stop, where the rotating half-wave plate is mounted, and a flat and telecentric focal plane suitable for the TES arrays. This configuration provides a 4° field of view for each focal plane with Strehl ratios of at least 0.966 at all frequencies across the entire field of view, and a Strehl ratio better than 0.991 across the full field of view for 150 GHz. To enable CMB observations to be made in four distinct frequency bands the incident light will be filtered, and different frequencies fed to different parts of the four focal planes. A reflecting metal-mesh low-pass filter with an edge at ~ 510 GHz will be mounted near the aperture stop of the system. The dichroic filter has

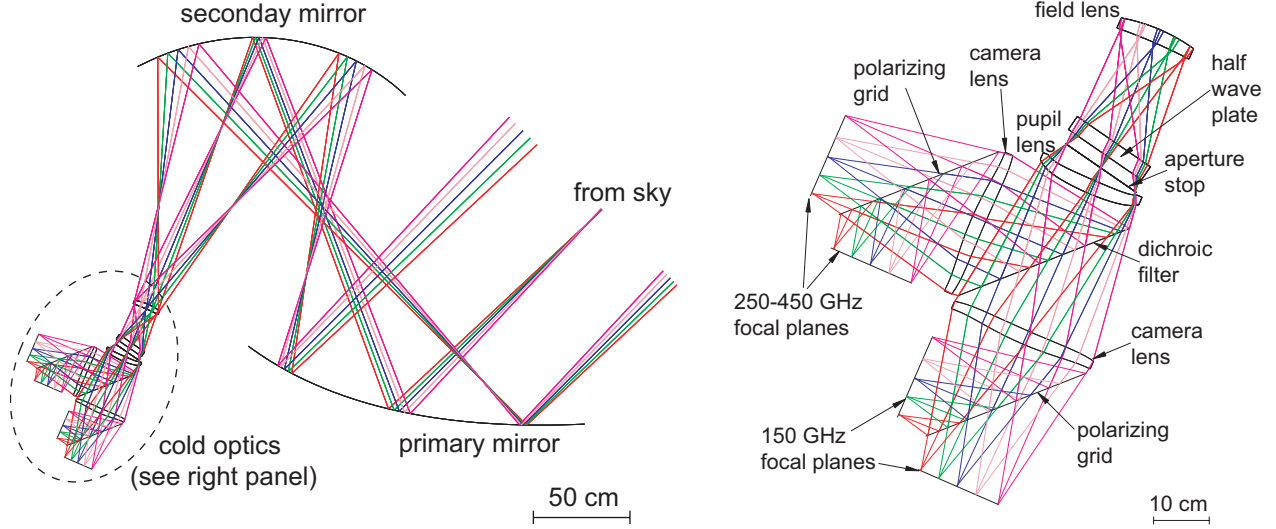


Figure 5. Left panel: The 1.5 m Dragone telescope provides 8 arcminute beams at 150 GHz. Light is coupled from the telescope to the cold optics, seen in close up on the right. Right panel: The cold optics image two perpendicular polarization components from each of the four frequencies onto four focal planes.

an edge at ~ 210 GHz, and acts as a low-pass filter in transmission and a high-pass filter in reflection. Two focal planes with up to a total of 660 detectors that are fed by light transmitted by this filter are allocated for the 150 GHz detectors. The other two focal planes with up to a total of 660 detectors are allocated for the three higher frequency bands. For each of the frequency bands, bandpass filters mounted in front of the focal plane will define the exact band shape. The capacitive inductive meshes of these filters are embedded in a transmissive polymer giving them mechanical rigidity even when cut to non-circular shapes. This flexibility allows us to use different parts of a given focal plane for different frequency bands.

Both silicon and high density polyethylene (HDPE) are commercially available at the sizes required for the lenses. Silicon and HDPE have indices of refraction of 3.416 and 1.567 at mm-wavelengths,^{44–47} which would give rise to coefficients of reflection of 30% and 4%, and to an absorption of 8% and 23% respectively at 150 GHz. We plan to coat either type of lens with an anti-reflection coating but the challenge is to develop a broad-band coating that adheres to the lens without causing damage when cooled to cryogenic temperatures. There is great interest in solving this problem in the larger CMB community because many experiments, including ACT, SPT, QUIET, BICEP, and perhaps a NASA CMB polarimetry satellite will need this technology.

Light will be coupled to the TES array by an array of smooth-walled conical horns. The use of a horn array places the detectors inside a Faraday cage where they are shielded from electromagnetic interference which may enter the cryostat window. The horns will have $1.7 F \lambda$ diameter entrance apertures at 150 GHz which allows 330 detectors to fill the 4° field-of-view of the EBEX telescope. The array will be fed at $F = 1.9$, giving a 6.5 mm horn aperture at 150 GHz, closely matching the bolometer spacing in the TES array.

The horn array will be made in two parts. A top section which is an array of conical holes, and a lower section an array of cylindrical holes acting as waveguides. Sandwiched between the two is a Cryoperm plate, also with holes in it (Fig. 6, left panel). This plate is the top plate of a large Cryoperm box which encloses the TES array and the SQUID detectors, which are located inside an additional smaller Cryoperm box at 4 K on the cryostat cold plate below the TES array. Each box attenuates external magnetic fields by more than two orders of magnitude which is necessary to avoid spurious signals in the SQUIDS and TES due to magnetic pickup from the half-wave plate rotation mechanism (Sec. 3.1.3). We calculate that with this magnetic shielding the spurious signal induced in the SQUID will be a factor of 300 smaller than the level of detector noise, while the signal in the TES is an additional factor of 2 smaller. The horn array and large Cryoperm box are connected to the 4 K cold plate of the cryostat and separated by a small gap from the TES array at 300 mK.

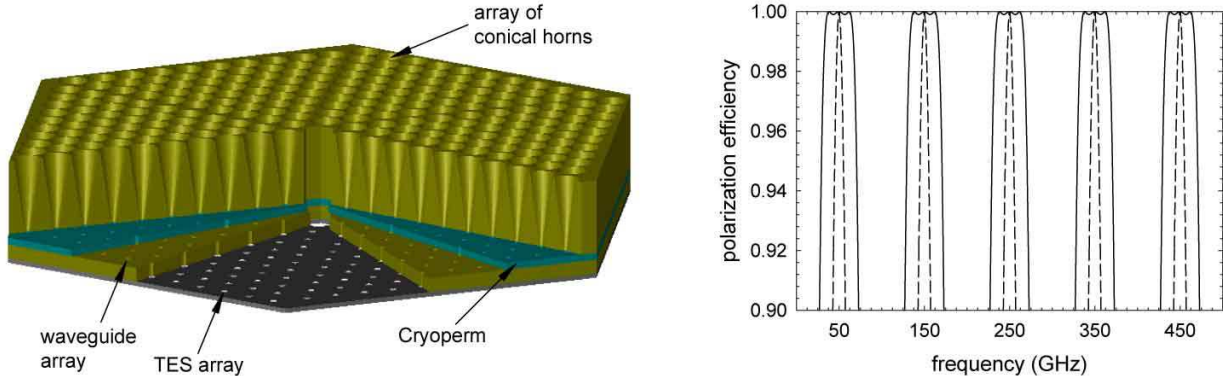


Figure 6. Left panel: Coupling light to the TES array with an array of conical horns and waveguides separated by a high permeability Cryoperm magnetic shield. The horns, shield, and waveguides are held at 4 K and the TES array at 300 mK. Right panel: Predicted efficiency of a stack of one (dashed line) and three (solid line) HWP as a function of frequency. For the 2.84 cm thick AHWP, each 0.946 cm plate is optimized as a single HWP for a frequency of 50 GHz. The efficiency function has the same shape and therefore the same bandwidth near the odd-harmonic peaks of 50 GHz.

3.1.3. Polarimetry

EBEX will use a combination of a rotating half-wave plate (HWP) and a fixed polarizing grid to modulate the polarization signal because this technique provides strong discrimination against systematic errors. To date all successful non-interferometric measurements of IR and mm-wave polarization have used a HWP to modulate the polarization signal. Examples include the Minnesota Infrared Polarimeter,⁴⁸ Stokes,⁴⁹ Millipol,⁵⁰ and SCUBA.⁵¹ The majority of bolometric CMB polarimeters will use a HWP.⁵²⁻⁵⁴

In EBEX the HWP will be rotated at a frequency of $f_0 = 20$ Hz which will modulate the polarization at $4f_0 = 80$ Hz. The combination of scanning the sky with the telescope at 1.8°s^{-1} and the rotation of the HWP puts the signal in 15 Hz wide sidebands around $4f_0$. This frequency is well below the ~ 160 Hz 3 dB bandwidth of the TES with a 1 ms time constant. We will maintain a polarization efficiency that is larger than 95% over a 40 GHz bandwidth for each of the four bands by employing an achromatic HWP (AHWP). The AHWP is made of a stack of three HWP's the middle one of which is rotated by 57.5° with respect to the aligned outer plates. The thickness of each HWP is optimized for a frequency of 50 GHz. Figure. 6, right panel, shows the predicted polarization efficiency for such a stack. Achromatic HWP's have been used in the past at the IR and optical wavelengths.^{48, 55, 56}

The use of a HWP as a polarization modulation provides the following important advantages in discrimination against systematic errors:

- Each detector makes independent measurements of T , Q , and U Stokes parameters for each pixel on the sky. No detector differencing is required. All schemes that rely on detector differencing are prone to errors or increased noise arising from, (a) uncertainty in the difference in gain between the detectors, (b) differences in beam pattern (if the detectors do not share the same light train), (c) difference in absolute calibration, and (d) difference in noise level between the detectors.
- Signals reside in relatively narrow and well defined sidebands around $4f_0$, where f_0 is the HWP modulation frequency. Spurious signals at all other frequency bands, including spurious effects that might arise from modulation at f_0 , are rejected.
- Sky signals are constrained to a band of frequencies that is much higher than the expected $\lesssim 1$ Hz knee in the $1/f$ noise spectrum of the detectors.
- Sources of instrumental polarization that are on the detector side of the HWP give rise to systematic effects that do not modulate with the HWP rotation and therefore do not affect the signals from the sky.
- Sources of instrumental polarization that are on the sky side of the HWP are very stable. Therefore they give rise to a stable signal at 80 Hz. A notch filter with a width of ~ 0.1 Hz removes such signals without affecting the signals from the sky.

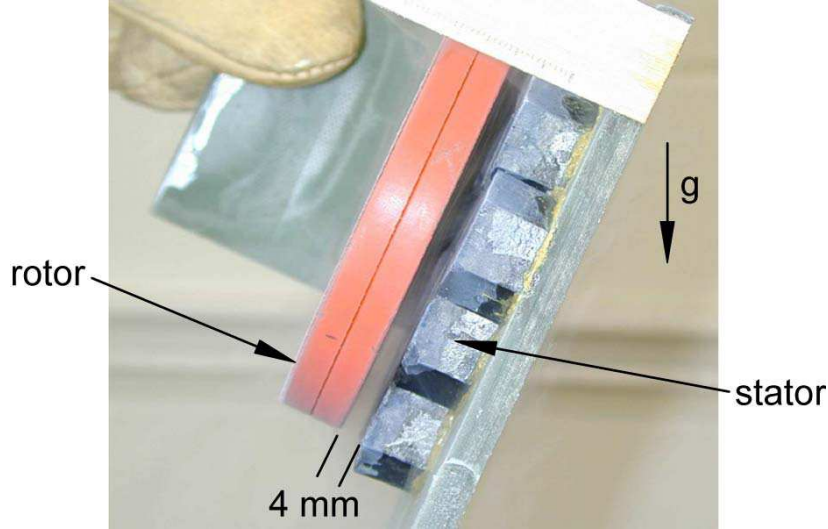


Figure 7. The superconducting magnetic bearing consists of a ring shaped magnet (rotor) and tiles of YBCO (stator) which are superconducting at temperatures below ~ 90 K. The HWP (not shown) is mounted inside the ring magnet. At temperatures above T_c the rotor is held by mechanical means above the stator. At temperatures below T_c the mechanical constraints are removed and the rotor maintains its position with respect to the stator *irrespective of the orientation of the acceleration vector due to gravity*. In this picture the stator was cooled to liquid nitrogen temperature with the rotor mechanically spaced ~ 4 mm above the tiles. Once cooled the spacing constraints were removed, the configuration lifted from the liquid nitrogen and the rotor was set spinning. The bearing was then abruptly tilted by $\sim 70^\circ$ with respect to the gravity vector. No change in the relative orientation of the rotor and stator and no oscillations of the rotor were observed. Stiff spring constants of $2.0 \times 10^3 \text{ Nm}^{-1}$ and $4.2 \times 10^3 \text{ Nm}^{-1}$ have been measured in the radial and axial directions, and the oscillation amplitude at the SMB characteristic frequency is less than $10 \mu\text{m}$.⁶¹

We are currently investigating a number of options for rotating the HWP. One option is to mount the HWP on a high-temperature superconducting magnetic bearing (SMB) turned with an induction motor (Fig. 7). Bolometers are sensitive to microphonic pickup and the SMB technique completely eliminates stick-slip friction, which is the primary source of microphonic noise in mechanical bearings. SMBs have been operating for many years^{57–60} and have been shown to reduce friction in bearings by more than 4 orders of magnitude. We plan to measure the noise properties and systematic effects associated with the SMB rotation mechanism. If the SMB is shown to be unsuitable then we have already demonstrated with the MAXIPOL experiment that through the use of special materials, such as vespel, teflon, or rulon, it is possible to reduce microphonic noise associated with mechanical bearings to the level appropriate for measurements of the E-mode polarization.⁵³ Since TES should have substantially less sensitivity to microphonic noise than thermistor bolometers³⁵ used in MAXIPOL, mechanical bearings may be suitable for a B-mode polarization experiment such as EBEX. In the unlikely event that neither of these techniques is suitable we will simply step-and-integrate with the HWP.

3.2. Control of Systematic Errors

The B-mode signal either from inflation or from lensing is expected to appear at the $\sim 0.1 \mu\text{K}$ level at a maximum (Fig. 1, left panel) and therefore a command of the sources of systematic errors is critical. We have checked that EBEX can meet specific goals that are necessary for extraction of the B-mode signal. Hu et al.⁶² have set benchmarks for the level of residual systematic errors in an experiment attempting to extract a B-mode signal with a given amplitude. The benchmarks calculated for EBEX for detecting an amplitude that is a *factor of five lower* than EBEX's 2σ upper limit are given in Table 2. EBEX calibration uncertainty in Stokes Q and U parameters is expected to be 1% – lower than the 6% benchmark, and we expect a maximum level of QU mixing of 0.8% at the edge of the focal plane. We expect a pointing uncertainty that is about a factor of ~ 3 smaller than the benchmark for 8 arcminute beams. In-flight measurements of Venus (Jupiter) will provide the shape parameters of the beam at each polarization state to an accuracy of 0.2% (0.1%) of the FWHM of the beam.

Table 2. Types of systematic uncertainties and residual uncertainty benchmarks for EBEX in order to detect a B-mode signal that is five times smaller than EBEX 2σ upper limit (following Hu et al.⁶²). These benchmarks represent residual uncertainties after all known corrections have been applied. The calibration term is the accuracy with which the TES bolometer response must be calibrated, and the QU term sets a limit on the allowable level of mixing between the Q and U polarization states caused by the telescope and optics. The pointing, monopole and dipole terms correspond to uncertainties in the pointing, in the size of beams in two orthogonal polarization states, and in the alignment of these beams, respectively, expressed as a fraction of the beam size. The quadrupole corresponds to uncertainty in the beam differential ellipticity.

Type	Calibration	QU	Pointing	Monopole	Dipole	Quadrupole
Unit	(%)	(%)	fraction of beam			diff. ell.
Level	6.4	1.6	0.11	0.002	0.007	0.017

We have designed these planet scans to achieve the benchmark required by the monopole term of Table 2. The dipole and differential ellipticity benchmarks are less restrictive and will already be satisfied by the planet scans.

4. CONCLUSIONS

EBEX will measure the CMB temperature and polarization anisotropy on angular scales from 8 arcminutes to 15° , thus finding, or setting a substantially improved limit, on the IGB signal of inflation. To achieve this EBEX will accurately characterize the foreground signal from Galactic dust which will also provide the CMB community with critical information about the polarized dust fraction and orientation as a function of frequency. EBEX should also detect the predicted, but as yet undetected, gravitational lensing of CMB radiation and significantly improve measurements of many cosmological parameters.

REFERENCES

1. A. A. Penzias and R. W. Wilson, “A Measurement of Excess Antenna Temperature at 4080 Mc/s.,” *Ap. J.* **142**, pp. 419–421, July 1965.
2. J. C. Mather, E. S. Cheng, D. A. Cottingham, R. E. Eplee, D. J. Fixsen, T. Hewagama, R. B. Isaacman, K. A. Jensen, S. S. Meyer, P. D. Noerdlinger, S. M. Read, L. P. Rosen, R. A. Shafer, E. L. Wright, C. L. Bennett, N. W. Boggess, M. G. Hauser, T. Kelsall, S. H. Moseley, R. F. Silverberg, G. F. Smoot, R. Weiss, and D. T. Wilkinson, “Measurement of the cosmic microwave background spectrum by the COBE FIRAS instrument,” *Ap. J.* **420**, pp. 439–444, Jan. 1994.
3. D. N. Spergel, L. Verde, H. V. Peiris, E. Komatsu, M. R.olta, C. L. Bennett, M. Halpern, G. Hinshaw, N. Jarosik, A. Kogut, M. Limon, S. S. Meyer, L. Page, G. S. Tucker, J. L. Weiland, E. Wollack, and E. L. Wright, “First-Year Wilkinson Microwave Anisotropy Probe (WMAP) Observations: Determination of Cosmological Parameters,” *Ap. J. Suppl.* **148**, pp. 175–194, Sept. 2003.
4. M. Tegmark, M. Strauss, M. Blanton, K. Abazajian, S. Dodelson, H. Sandvik, X. Wang, D. Weinberg, I. Zehavi, N. Bahcall, F. Hoyle, D. Schlegel, R. Scoccimarro, M. Vogeley, A. Berlind, T. Budavari, A. Connolly, D. Eisenstein, D. Finkbeiner, J. Frieman, J. Gunn, L. Hui, B. Jain, D. Johnston, S. Kent, H. Lin, R. Nakajima, R. Nichol, J. Ostriker, A. Pope, R. Scranton, U. Seljak, R. Sheth, A. Stebbins, A. Szalay, I. Szapudi, Y. Xu, and . others, “Cosmological parameters from SDSS and WMAP,” *ArXiv Astrophysics e-prints*, Oct. 2003. astro-ph/0310723.
5. J. M. Kovac, E. M. Leitch, C. Pryke, J. E. Carlstrom, N. W. Halverson, and W. L. Holzapfel, “Detection of polarization in the cosmic microwave background using DASI,” *Nature* **420**, p. 772, December 2002. astro-ph/0209478.
6. E. M. Leitch, J. M. Kovac, C. Pryke, J. E. Carlstrom, N. W. Halverson, W. L. Holzapfel, B. Reddall, and E. S. Sandberg, “Measurement of polarization with the degree angular scale interferometer,” *Nature* **420**, p. 763, December 2002. astro-ph/0209476.

7. A. Kogut, D. N. Spergel, C. Barnes, C. L. Bennett, M. Halpern, G. Hinshaw, N. Jarosik, M. Limon, S. S. Meyer, L. Page, G. S. Tucker, E. Wollack, and E. L. Wright, “First-Year Wilkinson Microwave Anisotropy Probe (WMAP) Observations: Temperature-Polarization Correlation,” *Ap. J. Suppl.* **148**, pp. 161–173, Sept. 2003. astro-ph/0302213.
8. W. Hu and M. White, “A new test of inflation,” *Phys. Rev. Lett.* **77**, p. 1687, Aug. 1996.
9. D. N. Spergel and M. Zaldarriaga, “Cosmic microwave background polarization as a direct test of inflation,” *Phys. Rev. Lett.* **79**, p. 2180, 1997.
10. H. V. Peiris, E. Komatsu, L. Verde, D. N. Spergel, C. L. Bennett, M. Halpern, G. Hinshaw, N. Jarosik, A. Kogut, M. Limon, S. S. Meyer, L. Page, G. S. Tucker, W. E., and W. E. L., “First-Year Wilkinson Microwave Anisotropy Probe (WMAP) Observations: Implications For Inflation,” *Ap. J. Suppl.* **148**, pp. 213–232, 2003.
11. A. H. Guth, “Inflationary universe: A possible solution to the horizon and flatness problems,” *Phys. Rev. D.* **23**, pp. 347–356, Jan. 1981.
12. A. D. Linde, “A new inflationary universe scenario: A possible solution of the horizon, flatness, homogeneity, isotropy and primordial monopole problems,” *Phys. Lett.* **B108**, pp. 389–393, 1982.
13. A. Albrecht and P. J. Steinhardt, “Cosmology for grand unified theories with radiatively induced symmetry breaking,” *Phys. Rev. Lett.* **48**, pp. 1220–1223, 1982.
14. K. Sato, “First-order phase transition of a vacuum and the expansion of the Universe,” *MNRAS* **195**, pp. 467–479, May 1981.
15. V. F. Mukhanov and G. V. Chibisov, “Quantum fluctuations and a nonsingular universe,” *JETP Letters* **33**, pp. 532–535, May 1981.
16. S. W. Hawking, “The development of irregularities in a single bubble inflationary universe,” *Phys. Lett. B* **115**, pp. 295–297, 1982.
17. A. H. Guth and S. Pi, “Fluctuations in the new inflationary universe,” *Phys. Rev. Lett.* **49**, pp. 1110–1113, Oct. 1982.
18. A. A. Starobinsky, “Dynamics of phase transition in the new inflationary universe scenario and generation of perturbations,” *Phys. Lett.* **B117**, pp. 175–178, 1982.
19. A. A. Starobinskii, “The perturbation spectrum evolving from a nonsingular initially De-Sitter cosmology and the microwave background anisotropy,” *Soviet Astronomy Letters* **9**, pp. 302–+, June 1983.
20. J. M. Bardeen, P. J. Steinhardt, and M. S. Turner, “Spontaneous creation of almost scale-free density perturbations in an inflationary universe,” *Phys. Rev. D.* **28**, p. 679, Aug. 1983.
21. V. F. Mukhanov, F. A. Feldman, and R. H. Brandenberger, “Theory of cosmological perturbations,” *Phys. Reports* **215**, pp. 203–333, June 1992.
22. V. A. Rubakov, M. V. Sazhin, and A. V. Veryaskin, “Graviton creation in the inflationary universe and the grand unification scale,” *Phys. Lett. B.* **115**, pp. 189–192, Sept. 1982.
23. L. P. Grishchuk, “Amplification of gravitational waves in an isotropic universe,” *Sov. Phys. JETP* **40**, pp. 409–415, 1975.
24. L. F. Abbott and M. B. Wise, “Constraints on generalized inflationary cosmologies,” *Nuclear Physics B* **244**, pp. 541–+, Oct. 1984.
25. M. Kamionkowski, A. Kosowsky, and A. Stebbins, “A Probe of Primordial Gravity Waves and Vorticity,” *Phys. Rev. Lett.* **78**, pp. 2058–2061, Mar. 1997. astro-ph/9609132.
26. U. Seljak and M. Zaldarriaga, “Signature of Gravity Waves in the Polarization of the Microwave Background,” *Phys. Rev. Lett.* **78**, pp. 2054–2057, Mar. 1997. astro-ph/9609169.
27. M. Kamionkowski and A. Loeb, “Getting around cosmic variance,” *Phys. Rev. D.* **56**, p. 4511, Oct. 1997.
28. M. Zaldarriaga and U. Seljak, “All-sky analysis of polarization in the microwave background,” *Phys. Rev. D.* **55**, pp. 1830–1840, 1997.
29. C. Baccigalupi, “Cosmic microwave background polarisation: foreground contrast and component separation,” *New Astronomy Review* **47**, pp. 1127–1134, Dec. 2003.
30. D. Ball, (NSBF Head of Operations) 2004. Private communication: Average length Antarctica balloon flight of 14 days.
31. C. Baccigalupi 2004. Private communication.

32. S. Hanany and P. Rosenkranz, "Polarization of the atmosphere as a foreground for cosmic microwave background polarization experiments," *New Astronomy Review* **47**, pp. 1159–1165, Dec. 2003.
33. B. Keating, P. Timbie, P. Polnarev, and J. Steinberger, "Large angular scale polarization of the cosmic microwave background and the feasibility of its detection," *Ap. J.* **496**, p. 580, 1998.
34. M. Zaldarriaga and U. Seljak, "Gravitational lensing effect on cosmic microwave background polarization," *Phys. Rev. D.* **58**, p. 23003 (6 pages), July 1998.
35. D. Schwan, F. Bertoldi, S. Cho, M. Dobbs, R. Guesten, N. W. Halverson, W. L. Holzapfel, E. Kreysa, T. M. Lanting, A. T. Lee, M. Lueker, J. Mehl, K. Menten, D. Muders, M. Myers, T. Plagge, A. Raccanelli, P. Schilke, P. L. Richards, H. Spieler, and M. White, "APEX-SZ a Sunyaev-Zel'dovich galaxy cluster survey," *New Astronomy Review* **47**, pp. 933–937, Dec. 2003.
36. <http://astro.uchicago.edu/spt>.
37. A. T. Lee, P. L. Richards, S. W. Nam, B. Cabrera, and K. D. Irwin, "A Superconducting Bolometer with Strong Electrothermal Feedback," *Applied Physics Letters* **69**, pp. 1801–1803, Sept. 1996.
38. S. Lee, J. M. Gildemeister, W. Holmes, A. T. Lee, and P. L. Richards, "Voltage-Biased Superconducting Transition-Edge Bolometer with Strong Electrothermal Feedback Operated at 370 mK," *Appl. Optics* **37**, pp. 3391–3397, June 1998.
39. J. M. Gildemeister, A. T. Lee, and P. L. Richards, "A Fully Lithographed Voltage-biased Superconducting Spiderweb Bolometer," *Applied Physics Letters* **74**, pp. 868–870, Feb. 1999.
40. J. M. Gildemeister, A. T. Lee, and P. L. Richards, "Monolithic Arrays of Absorber-coupled Voltage-biased Superconducting Bolometers," *Applied Physics Letters* **77**, pp. 4040–4042, Dec. 2000.
41. J. M. Gildemeister, *Voltage-Biased Superconducting Bolometers for Infrared and mm-Waves*. PhD thesis, University of California, Berkeley, 2000.
42. J. Yoon, J. Clarke, J. M. Gildemeister, A. T. Lee, M. J. Myers, P. L. Richards, and J. T. Skidmore, "Single Superconducting Quantum Interference Device Multiplexer for Arrays of Low-Temperature Sensors," *Applied Physics Letters* **78**, pp. 371–373, Jan. 2001.
43. M. F. Cunningham, J. N. Ullom, T. Miyazaki, S. E. Labov, J. Clarke, T. M. Lanting, A. T. Lee, P. L. Richards, J. Yoon, and H. Spieler, "High-resolution operation of frequency-multiplexed transition-edge photon sensors," *Applied Physics Letters* **81**, pp. 159–161, July 2002.
44. J. R. Birch and Kong Fan Ping, "An interferometer for the determination of the temperature variation of the complex refraction spectra of reasonably transparent solids at near-millimetre wavelengths," *Infrared Physics* **24**, pp. 309–314, May 1984.
45. J. R. Birch, "Systematic errors in dispersive fourier transform spectroscopy in a non-vacuum environment," *Infrared Physics* **34**, pp. 89–93, 1993.
46. V. V. Parshin, R. Heidinger, B. A. Andreev, A. V. Gusev, and V. B. Shmagin, "Silicon as an advanced window material for high power gyrotrons," *Int. J. Infrared and Millimeter Waves* **16**, pp. 864–877, 1995.
47. M. N. Afsar and E. A. Nichol, "Millimeter wave complex refractive index, complex dielectric permittivity and loss tangent of extra high purity and compensated silicon," *Int. J. Infrared and Millimeter Waves* **15**, pp. 1181–1188, 1994.
48. T. J. Jones and D. Klebe, "A simple infrared polarimeter," *Proc. Ast. Soc. Pac.* **100**, pp. 1158–1161, Sept. 1988.
49. S. R. Platt, R. H. Hildebrand, R. J. Pernic, J. A. Davidson, and G. Novak, "100-micron array polarimetry from the Kuiper Airborne Observatory - Instrumentation, techniques, and first results," *Proc. Ast. Soc. Pac.* **103**, pp. 1193–1210, Nov. 1991.
50. R. W. Leach, D. P. Clemens, B. D. Kane, and R. Barvainis, "Polarimetric mapping of Orion using MILLIPOL - Magnetic activity in BN/KL," *Ap. J.* **370**, pp. 257–262, Mar. 1991.
51. A. G. Murray, R. Nartallo, C. V. Haynes, F. Gannaway, and P. A. R. Ade, "An Imaging Polarimeter for SCUBA," in *ESA SP-401: The Far Infrared and Submillimetre Universe*, pp. 405–+, 1997.
52. S. Church, P. Ade, J. Bock, M. Bowden, J. Carlstrom, K. Ganga, W. Gear, J. Hinderks, W. Hu, B. Keating, J. Kovac, A. Lange, E. Leitch, O. Mallie, S. Melhuish, A. Murphy, B. Rusholme, C. O'Sullivan, L. Piccirillo, C. Pryke, A. Taylor, and K. Thompson, "QUEST on DASI: A South Pole CMB polarization experiment," *New Astronomy Review* **47**, pp. 1083–1089, Dec. 2003.

53. B. R. Johnson, M. E. Abroe, P. Ade, J. Bock, J. Borrill, J. S. Collins, P. Ferreira, S. Hanany, A. H. Jaffe, T. Jones, A. T. Lee, L. Levinson, T. Matsumura, B. Rabii, T. Renbarger, P. L. Richards, G. F. Smoot, R. Stompor, H. T. Tran, and C. D. Winant, "MAXIPOL: a balloon-borne experiment for measuring the polarization anisotropy of the cosmic microwave background radiation," *New Astronomy Review* **47**, pp. 1067–1075, Dec. 2003. astro-ph/0308259.
54. <http://bolo.berkeley.edu/polarbear/>.
55. C. J. Koester, "Achromatic combinations of half-wave plates," *J. Opt. Soc. Am.* **49**, pp. 405–409, 1959.
56. S. Pancharatnam, "Achromatic combinations of birefringent plates," *Raman Research Inst. Bangalore, Memoir*, 1955.
57. A. Rivetti, G. Martini, R. Gorla, and S. Loreface, "Turbine flowmeter for liquid helium with the rotor magnetically levitated," *Cryogenics* **27**, pp. 8–11, 1987.
58. R. Decher, P. N. Peters, R. C. Sisk, E. W. Urban, M. Vlasse, and D. K. Rao, "High temperature superconducting bearing for rocket engine turbopumps," *Applied Superconductivity* **1**, pp. 1265–1278, 1993.
59. J. R. Hull, "Flywheels on a roll," *Spectrum, IEEE*. **34**, pp. 20–25, 1997.
60. Y. Zhang, Y. Postrekhin, K. B. Ma, and W. K. Chu, "Reaction wheel with HTS bearings for mini-satellite attitude control," *Supercond. Sci. Technol.* **15**, pp. 823–825, May 2002.
61. S. Hanany, T. Matsumura, B. Johnson, T. Jones, J. R. Hull, and K. B. Ma, "A cosmic microwave background radiation polarimeter using superconducting bearings," *IEEE Transactions on Applied Superconductivity* **13**, pp. 2128–2133, 2003.
62. W. Hu, M. M. Hedman, and M. Zaldarriaga, "Benchmark parameters for CMB polarization experiments," *Phys. Rev. D*. **67**, pp. 043004–+, Feb. 2003. astro-ph/0210096.